

## Magnetic properties of a spin-2 antiferromagnet with metal-radical hybrid spins

Y. Iwasaki,<sup>1,\*</sup> T. Okabe,<sup>1</sup> N. Uemoto,<sup>1</sup> Y. Kono,<sup>1</sup> Y. Hosokoshi,<sup>1</sup> S. Nakamura,<sup>2</sup> S. Kittaka,<sup>3</sup> T. Sakakibara,<sup>3</sup> M. Hagiwara,<sup>4</sup> T. Kawakami,<sup>5</sup> and H. Yamaguchi<sup>1,†</sup>

<sup>1</sup>Department of Physical Science, Osaka Prefecture University, Osaka 599-8531, Japan

<sup>2</sup>Nagoya Institute of Technology, Nagoya 466-8555, Japan

<sup>3</sup>Institute for Solid State Physics, The University of Tokyo, Chiba 277-8581, Japan

<sup>4</sup>Center for Advanced High Magnetic Field Science (AHMF), Graduate School of Science, Osaka University, Osaka 560-0043, Japan

<sup>5</sup>Department of Chemistry, Osaka University, Osaka 560-0043, Japan



(Received 4 February 2020; revised manuscript received 25 March 2020; accepted 21 April 2020; published 7 May 2020)

We present an  $S = 2$  antiferromagnet composed of a Mn-verdazyl complex  $[\text{Mn}(\text{hfac})_2][o\text{-Py-V-(4-F)}_2]$ . An analysis of the magnetic behavior reveals that the strong antiferromagnetic intramolecular interaction between spins on  $\text{Mn}^{2+}$  and the verdazyl radical forms an  $S = 2$  hybrid spin below approximately 100 K. In the low-temperature regions, the magnetic susceptibility and the specific heat indicate a phase transition to the three-dimensional order of the  $S = 2$  system. Below the transition temperature, the magnetization curve exhibits a metamagnetic phase transition. From the analysis of electron spin resonance modes, we evaluate the on-site biaxial anisotropy responsible for the anisotropic magnetic behavior.

DOI: [10.1103/PhysRevB.101.174412](https://doi.org/10.1103/PhysRevB.101.174412)

### I. INTRODUCTION

Organic radical materials have attracted attention since the discovery of the organic ferromagnet composed of the nitroxide-type radical [1–4]. Metal-radical complexes have been obtained by using mainly nitroxide-type radicals [5–9]. The strong metal-radical couplings in such complexes form not only polymer structures but also metal-radical hybrid spins in low-temperature regions [10–12]. The coordination chemistry of verdazyl radicals has also been intensively investigated [13–16] since the first complexes were reported in 1997 by Brook *et al.* [17].

We have developed material designs for quantum spin systems by using verdazyl radicals and realized various unconventional spin-1/2 systems [18–23]. As the next step in the material design, we have been developing the synthesis of verdazyl-based complexes by combination with 3d transition metals [24–27]. By forming metal-radical hybrid spins in the synthesized complexes, we progress toward the realization of more diverse spin systems with spins of  $S > 1/2$ . We have synthesized verdazyl-based complexes  $[\text{M}(\text{hfac})_2](o\text{-Py-V})$  ( $\text{M} = \text{Zn}, \text{Mn}$ ) [24,25], where hfac is 1,1,1,5,5,5-hexafluoroacetylacetonate and  $o\text{-Py-V}$  is 3-(2-pyridinyl)-1,5-diphenylverdazyl. The Zn-verdazyl complex  $[\text{Zn}(\text{hfac})_2](o\text{-Py-V})$  formed a spin-1/2 alternating chain. The crystal structure of the Mn-verdazyl complex  $[\text{Mn}(\text{hfac})_2](o\text{-Py-V})$  is isomorphous to that of  $[\text{Zn}(\text{hfac})_2](o\text{-Py-V})$ . An analysis of magnetic properties has demonstrated that the intramolecular antiferromagnetic (AF) interaction between spins on  $\text{Mn}^{2+}$  ( $S_{\text{Mn}} = 5/2$ ) and verdazyl

radicals ( $S_{\text{V}} = 1/2$ ) in  $[\text{Mn}(\text{hfac})_2](o\text{-Py-V})$  forms an  $S = 2$  hybrid spin below approximately 100 K. The corresponding intramolecular interaction  $J_{\text{intra}}$ , defined by the spin Hamiltonian  $\mathcal{H} = J_{\text{intra}} S_{\text{Mn}} \cdot S_{\text{V}}$ , is evaluated to be 325 K. Accordingly, in the low-temperature region, the magnetic properties are well explained by an  $S = 2$  alternation chain with a small on-site biaxial anisotropy evaluated by our electron spin resonance (ESR) analysis. These results demonstrate that our material design can change a spin-1/2 system to a spin-2 system by using metal-radical complexes. Experimentally, the ground-state properties of a spin-2 system still have not been verified in detail. The  $S = 2$  AF chain is a typical example, and its ground-state phase diagram has been discussed numerically [28–33].

Recently, we synthesized a verdazyl-based complex  $[\text{Zn}(\text{hfac})_2][o\text{-Py-V-(4-F)}_2]$  [34], where  $o\text{-Py-V-(4-F)}_2$  is 3-(2-pyridinyl)-1,5-bis(4-fluorophenyl)-verdazyl. *Ab initio* molecular orbital calculations indicate that three dominant intermolecular interactions,  $J_1, J_2$ , and  $J_3$ , form an  $S = 1/2$  Heisenberg honeycomb lattice, as shown in Fig. 1.  $J_1$  and  $J_2$  are AF, while  $J_3$  is ferromagnetic. The nonmagnetic hfac acts as a spacer between the two-dimensional (2D) honeycomb structures, and thus the interplane couplings are evaluated to be less than approximately 1/50 of  $J_1$  in absolute values. Actually, no phase transition to a magnetic ordered state is observed down to the extremely low-temperature region owing to its high two-dimensionality. The lattice distortion effects are examined by using a simplified honeycomb lattice with  $J_2 = |J_3|$ . A dimerlike lattice distortion, which causes a quantum phase transition to a gapped dimer phase at a critical distortion ratio [35–37], is expected in the range of  $0.8 < J_2/J_1 < 1.0$ . Furthermore, numerical studies on magnetic behavior have revealed that the lattice distortion in this compound does not affect the intrinsic properties of the  $S =$

\*iwasaki@ahmf.sci.osaka-u.ac.jp

†yamaguchi@p.s.osakafu-u.ac.jp

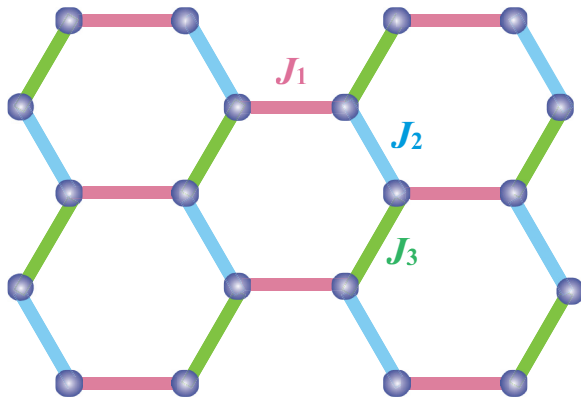


FIG. 1. Distorted honeycomb lattice composed of  $J_1$ ,  $J_2$ , and  $J_3$  in  $[\text{M}(\text{hfac})_2][o\text{-Py-V-(4-F)}_2]$  ( $\text{M} = \text{Zn}, \text{Mn}$ ).

$1/2$  honeycomb lattice. In the present compound,  $\text{Mn}^{2+}$  ions are coordinated instead of  $\text{Zn}^{2+}$ , and an effective  $S = 2$  honeycomb lattice is expected to be formed through Mn-verdazyl intramolecular interactions in low-temperature regions.

In this paper, we present a verdazyl-based complex forming an  $S = 2$  antiferromagnet. We synthesized single crystals of the Mn-verdazyl complex  $[\text{Mn}(\text{hfac})_2][o\text{-Py-V-(4-F)}_2]$ . Through analysis of the magnetic behavior, we reveal that the strong AF intramolecular interaction between spins on  $\text{Mn}^{2+}$  and the verdazyl radical forms an  $S = 2$  hybrid spin below approximately 100 K. In low-temperature regions, the magnetic susceptibility and specific heat indicate a phase transition to the 3D order. Below  $T_N$ , the magnetization curve exhibits a metamagnetic phase transition in the  $S = 2$  system. By analyzing the ESR modes, we evaluate the on-site biaxial anisotropy responsible for the anisotropic magnetic behavior.

## II. EXPERIMENTAL PROCEDURE

The synthesis of  $[\text{Mn}(\text{hfac})_2][o\text{-Py-V-(4-F)}_2]$ , whose molecular structure is shown in Fig. 2(a), was performed using a procedure similar to that for  $[\text{Zn}(\text{hfac})_2][o\text{-Py-V-(4-F)}_2]$  [34]. Recrystallization in acetonitrile yielded dark-green crystals. X-ray intensity data were collected using a Rigaku AFC-8R mercury CCD RA-micro7 diffractometer with graphite-monochromated  $\text{MoK}\alpha$  radiation and Japan Thermal Engineering XR-HR10K. The structure was solved by a direct method using SIR2004 [38] and was refined with SHELXL97 [39]. The structural refinement was carried out using anisotropic and isotropic thermal parameters for nonhydrogen atoms and hydrogen atoms, respectively. Magnetizations were measured using a commercial SQUID magnetometer (MPMS-XL, Quantum Design) with a  $^3\text{He}$  refrigerator down to approximately 0.5 K. The experimental result was corrected for the diamagnetic contribution  $-3.67 \times 10^{-4} \text{ emu mol}^{-1}$ , which was calculated using the Pascal method. The specific heat was measured with a commercial calorimeter (PPMS; Quantum Design) by a thermal relaxation method above 2.0 K and by an adiabatic method down to approximately 0.3 K. ESR measurements were performed utilizing a vector network analyzer (ABmm), a superconducting magnet (Oxford Instruments), and a homemade ESR cryostat at the

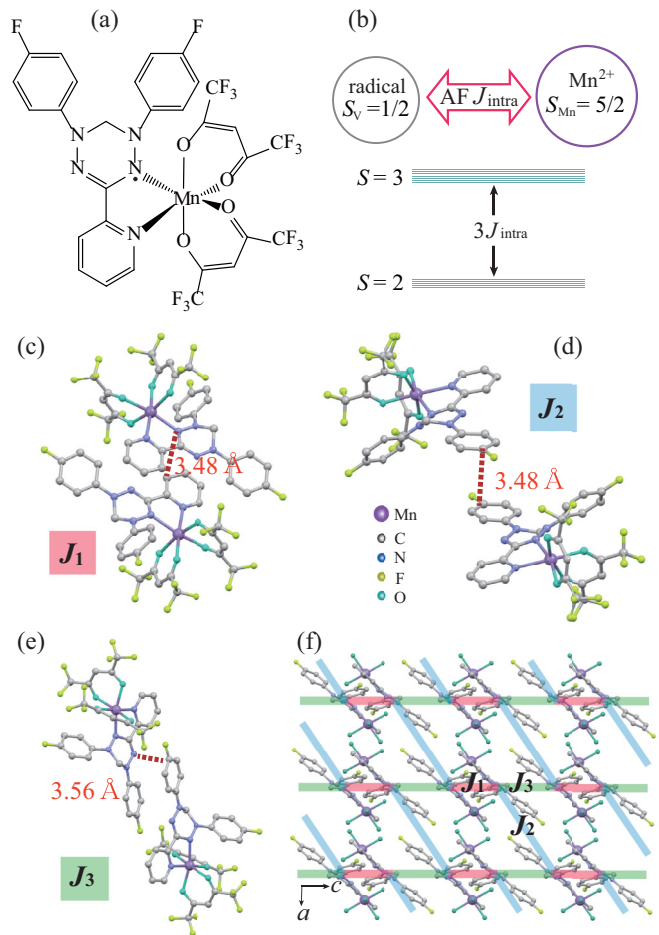


FIG. 2. (a) Molecular structure of  $[\text{Mn}(\text{hfac})_2][o\text{-Py-V-(4-F)}_2]$ . (b) Schematic of the intramolecular interaction between spins on  $\text{Mn}^{2+}$  and the verdazyl radical and resulting spin states. Molecular pairs associated with the exchange interactions (c)  $J_1$ , (d)  $J_2$ , and (e)  $J_3$ . Hydrogen atoms are omitted for clarity. (f) Crystal structure forming a 2D honeycomb lattice in the  $ac$  plane, in which each hfac in the molecule is omitted for clarity.

Center for Advanced High Magnetic Field Science, Osaka University.

## III. RESULTS AND DISCUSSION

### A. Crystal structure and magnetic model

The crystallographic data for  $[\text{Mn}(\text{hfac})_2][o\text{-Py-V-(4-F)}_2]$  are summarized in Table I. The radical center, which includes four N atoms, is directly bonded to a  $\text{Mn}^{2+}$  ion, as shown in Fig. 2(a). As in the case of  $[\text{Mn}(\text{hfac})_2](o\text{-Py-V})$ , with a similar coordination structure, it is expected that a strong intramolecular AF interaction  $J_{\text{intra}}$  between spins on  $\text{Mn}^{2+}$  ( $S_{\text{Mn}} = 5/2$ ) and the verdazyl radical ( $S_V = 1/2$ ) forms a Mn-verdazyl hybrid spin [25]. The strong AF  $J_{\text{intra}}$  leads to the large energy gap of  $3J_{\text{intra}}$  between the resultant spins of  $S = 2$  and 3, as shown in Fig. 2(b). As the lower states of  $S = 2$  are well separated from the excited states of  $S = 3$ , the  $[\text{Mn}(\text{hfac})_2][o\text{-Py-V-(4-F)}_2]$  molecule can be considered to have a Mn-verdazyl hybrid spin  $S = 2$  for  $T \ll 3J_{\text{intra}}$ . It is also expected that approximately 70% of the total spin density

TABLE I. Crystallographic data for  $[\text{Mn}(\text{hfac})_2][o\text{-Py-V-(4-F)}_2]$ .

Formula	$\text{C}_{29}\text{H}_{16}\text{F}_{14}\text{N}_5\text{O}_4\text{Mn}$	
Crystal system	Monoclinic	
Space group	$P2_1/c$	$P2_1$
Temperature (K)	RT	25(2)
Wavelength (Å)	0.7107	
$a$ (Å)	9.052(3)	8.813(4)
$b$ (Å)	32.508(12)	32.167(14)
$c$ (Å)	10.988(4)	10.903(5)
$\beta$ (deg)	92.278(4)	91.119(6)
$V$ (Å <sup>3</sup> )	3231(2)	3090(2)
$Z$	4	
$D_{\text{calc}}$ (g cm <sup>-3</sup> )	1.685	1.761
Total reflections	5322	9713
Reflections used	4373	7136
Parameters refined	478	955
$R [I > 2\sigma(I)]$	0.0621	0.0504
$R_w [I > 2\sigma(I)]$	0.1640	0.1118
Goodness of fit	1.046	1.004
CCDC	1 992 364	1 992 365

of  $S = 2$  is present on the Mn atom, whereas  $o\text{-Py-V-(4-F)}_2$  has approximately 30% of the total spin density of  $S = 2$  [25].

No direct correlation exists between the Mn atoms, and the nonmagnetic hfac functions as a spacer between molecular spins. Therefore, intermolecular magnetic interactions emerge through the overlap of molecular orbitals on the radical. The crystal structure at room temperature (RT) is isomorphous to that of  $[\text{Zn}(\text{hfac})_2][o\text{-Py-V-(4-F)}_2]$  [34]. Thus, the present Mn-verdazyl complex is also expected to form an  $S = 2$  distorted honeycomb lattice composed of three dominant interactions,  $J_1$ ,  $J_2$ , and  $J_3$ , as shown in Fig. 1. Figures 2(c)–2(e) show the molecular pairs associated with these interactions, which are related by an inversion center at RT. At 25 K, each molecular pair is composed of two crystallographically independent molecules owing to the disappearance of the inversion center. The N-C and C-C short contacts for the  $J_1$ ,  $J_2$ , and  $J_3$  interactions are 3.48, 3.48, and 3.56 Å, as shown in Figs. 2(c)–2(e), respectively. The three dominant interactions lead to the formation of a honeycomb lattice in the  $ac$  plane, as shown in Fig. 2(f). The exchange interactions between  $S = 2$  hybrid spins are obtained from the second-order perturbation treatment of interactions between  $S = 1/2$  spins on  $o\text{-Py-V-(4-F)}_2$ . Thus,  $J_1$ ,  $J_2$ , and  $J_3$  forming the  $S = 2$  honeycomb lattice are expected to be very weak in analogy with  $[\text{Mn}(\text{hfac})_2](o\text{-Py-V})$  [25].

As described below, the magnetic properties indicate that the actual values of the interactions between the hybrid spins are smaller than approximately 1 K. Considering the strong dependence on the calculation method and basis set in the molecular orbital calculation, it is difficult to evaluate such small exchange interactions with a reliable accuracy [40].

### B. Magnetic susceptibility

Figure 3 shows the temperature dependence of the magnetic susceptibility ( $\chi = M/H$ ) measured by using randomly oriented single crystals.  $\chi T$  decreases with decreasing temperature and becomes approximately constant at approxi-

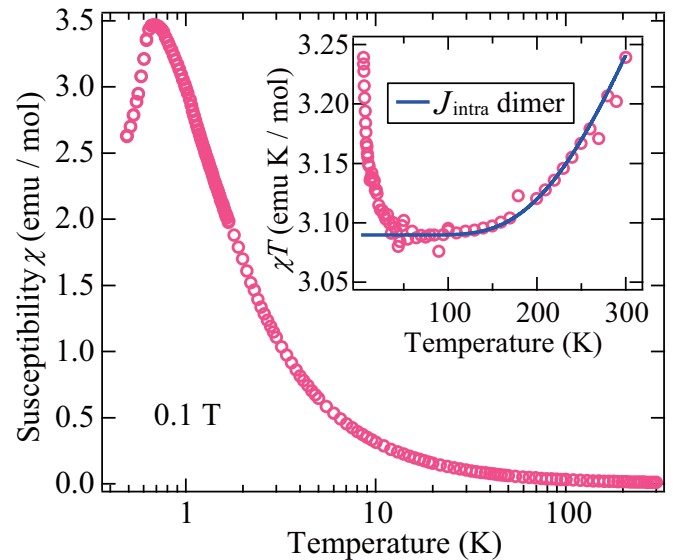


FIG. 3. Temperature dependence of the magnetic susceptibility ( $\chi = M/H$ ) of  $[\text{Mn}(\text{hfac})_2][o\text{-Py-V-(4-F)}_2]$  at 0.1 T for randomly oriented single crystals. Inset: Temperature dependence of  $\chi T$  for the high-temperature region. The solid line represents the calculated results for the  $S_{\text{Mn}}\text{-}S_{\text{V}}$  dimer coupled by  $J_{\text{intra}}$ .

mately 100 K, as shown in the inset in Fig. 3. The constant value of  $\chi T$  is close to the Curie constant of 3.0 emu · K/mol for noninteracting  $S = 2$  spins, which evidences the formation of the hybrid spin  $S = 2$  through the strong AF  $J_{\text{intra}}$ . We calculated  $\chi T$  for the  $S_{\text{Mn}}\text{-}S_{\text{V}}$  dimer coupled through  $J_{\text{intra}}$  and obtained an impressive agreement between the experiment and the calculation above approximately 100 K by using  $J_{\text{intra}}/k_B = 330$  K and  $g = 2.03$ . The evaluated  $J_{\text{intra}}$  is very close to that in  $[\text{Mn}(\text{hfac})_2](o\text{-Py-V})$  [25]. We observed a discontinuous change in  $\chi$  at approximately 0.63 K, which is associated with a phase transition to a 3D magnetic order because of the weak but finite 3D couplings.

### C. Specific heat

The experimentally determined specific heat  $C_p$  at zero field exhibits a  $\lambda$ -type sharp peak associated with the phase transition to the 3D order at  $T_N = 0.63$  K, as shown in Fig. 4(a). Although the lattice contributions are not subtracted from  $C_p$ , the magnetic contributions are expected to be dominant in the low-temperature regions below  $T_N$ , as observed for other verdazyl-based materials [18–20].

The entropy  $S_p$  obtained through integration of  $C_p/T$  shows that the change associated with the phase transition almost corresponds to one-third of the total magnetic entropy of  $S = 2$  ( $1/3R \ln 5 \simeq 4.5$  J/mol K), as shown in the inset in Fig. 4(a). Therefore, the observed phase transition originates from the magnetic order of the  $S = 2$  hybrid spin. The present spin system indeed has a 2D character, yielding a sufficient development of a short-range order in the 2D honeycomb plane above  $T_N$ .

By applying a magnetic field of 0.3 T, the phase transition peak disappears for  $H||b$ , whereas the peak temperature slightly shifts to the lower-temperature region for  $H||c$ , as

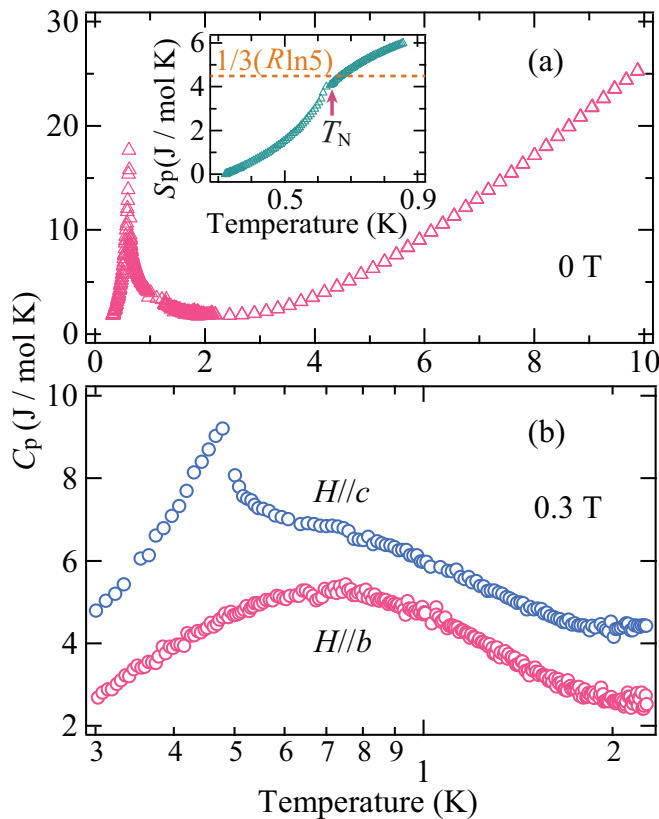


FIG. 4. Specific heat of  $[\text{Mn}(\text{hfac})_2][o\text{-Py-V-(4-F)}_2]$  at (a) 0 T and (b) 0.3 T for  $H||b$  and  $H||c$ . The values for  $H||c$  have been shifted up by 2.0 J/mol K. Inset: Low-temperature part of the evaluated entropy at 0 T. The arrow indicates the phase transition temperature  $T_N$ .

shown in Fig. 4(b). These results are associated with a large magnetic anisotropy. As shown in the next subsection, the magnetization curve for  $H||b$  is almost fully polarized at 0.3 T, while the magnetization curve for  $H||c$  still increases gradually. Accordingly, a few degrees of freedom can cause magnetic order for  $H||b$  at 0.3 T, which indicates a large easy-axis anisotropy along the  $b$  axis.

#### D. Magnetization curve

We describe the magnetization curves in a low-temperature region below  $T_N$ . The measured saturation magnetization  $M_{\text{sat}} \sim 4.0\mu_B/\text{f.u.}$  is consistent with that theoretically expected in the  $S = 2$  system, as shown in Fig. 5. We observed a distinct metamagnetic phase transition at  $H_c \sim 0.12$  T for  $H||b$ , while the magnetization curve for  $H||c$  apparently exhibits a monotonic increase, as shown in Fig. 5. This anisotropic behavior is consistent with the field dependence of the specific heat, and the metamagnetic phase transition demonstrates the presence of an easy-axis anisotropy sufficiently larger than the exchange interactions forming the  $S = 2$  honeycomb lattice.

#### E. Electron spin resonance

We performed ESR measurements to evaluate the expected magnetic anisotropy. Figure 6(a) shows the temperature de-

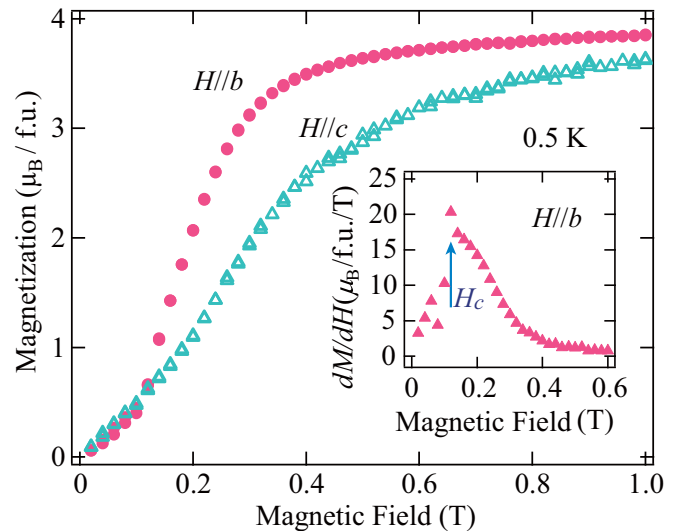


FIG. 5. Magnetization curve of  $[\text{Mn}(\text{hfac})_2][o\text{-Py-V-(4-F)}_2]$  at 0.5 K for  $H||b$  and  $H||c$ . Inset: Field derivative of the magnetization curve ( $dM/dH$ ) for  $H||b$  in the vicinity of  $H_c$  indicated by the arrow.

pendence of the resonance fields at 91.5 GHz for  $H||b$ . In high-temperature regions, the transitions between the lower  $S = 2$  states are not clearly observed because of the thermal excitation. With decreasing temperature, the resonance signals originating from the transitions between  $S = 2$  states are enhanced. Considering the energy scale of the exchange interactions forming the  $S = 2$  honeycomb lattice, the observed

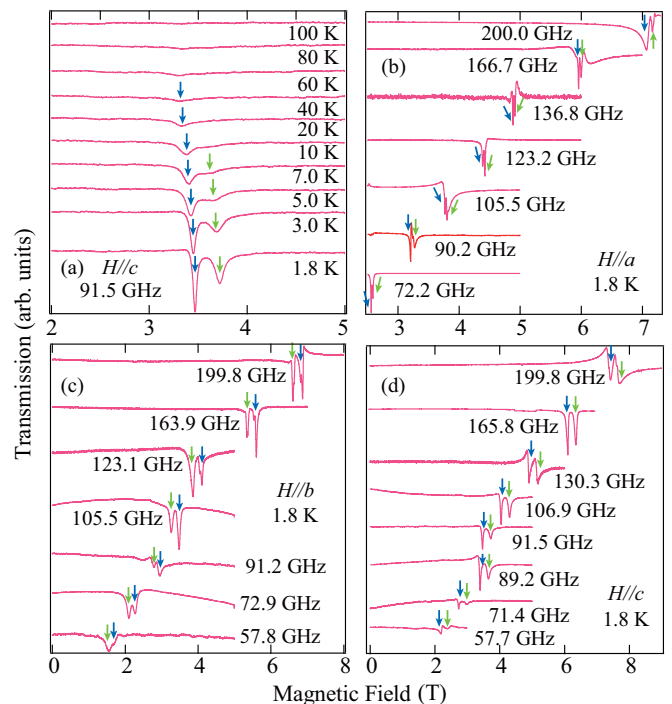


FIG. 6. (a) Temperature dependence of ESR absorption spectra of  $[\text{Mn}(\text{hfac})_2][o\text{-Py-V-(4-F)}_2]$  at 91.5 GHz for  $H||c$ . Representative frequency dependence of ESR absorption spectra at 1.8 K for (b)  $H||a$ , (c)  $H||b$ , and (d)  $H||c$ . Green and blue arrows indicate the resonance fields for site 1 and site 2, respectively.

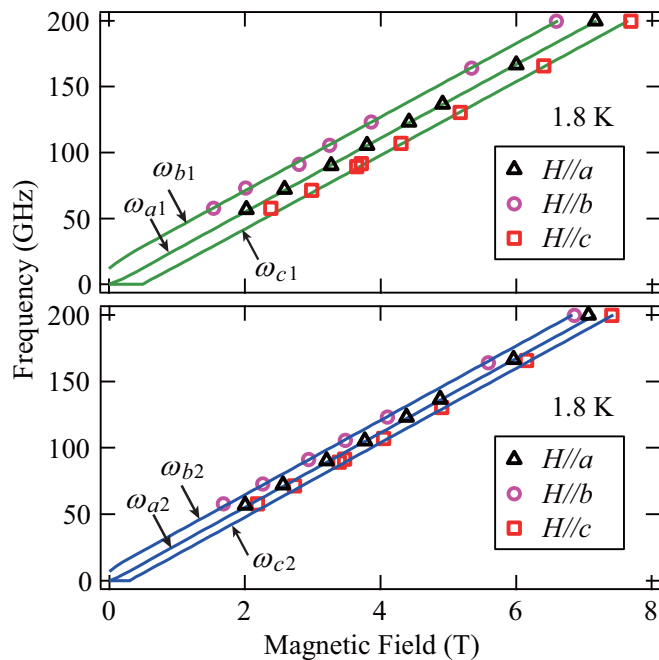


FIG. 7. Frequency-field diagram of the resonance fields at 1.8 K for (a) site 1 and (b) site 2. Solid lines indicate the calculated paramagnetic resonance modes of the  $S = 2$  hybrid spin with on-site biaxial anisotropy, which correspond to the transitions indicated by the arrows in the energy branches in Fig. 8.

signals are considered as the paramagnetic resonance of the  $S = 2$  hybrid spin. In low-temperature regions, two signals appear owing to the slightly different mean fields in two crystallographically independent molecules in the low-temperature crystal structure, as observed for  $[\text{Mn}(\text{hfac})_2](o\text{-Py-V})$  [25].

Figures 6(b)–6(d) show the frequency dependences of the resonance fields at 1.8 K, for  $H\parallel a$ ,  $H\parallel b$ , and  $H\parallel c$ , respectively. Signal splitting is observed in all magnetic field directions. We distinguished the two signals by considering the contribution of the anisotropy for each field direction, as shown by the two types of arrows in Figs. 6(b)–6(d), and plotted the resonance fields in the frequency-field diagram as site 1 and site 2, as shown in Figs. 7(a) and 7(b). Clear differences are observed between the three field directions for both sites.

Further, we evaluate the magnetic anisotropy by using the frequency dependence of the ESR signals. We consider the on-site biaxial anisotropy as  $\mathcal{H} = D(S_z)^2 + E\{(S_x)^2 - (S_y)^2\} + g\mu_B H S_i$ , where  $\mu_B$  is the Bohr magneton,  $H$  is the external magnetic field, the  $x$ ,  $y$ , and  $z$  axes correspond to the  $b \times c$ ,  $c$ , and  $b$  directions, respectively, and  $S$  is the  $S = 2$  spin operator. Since the anisotropy of the  $g$  factor in the present compound is expected to be small, we assumed  $g = 2.0$  for the resonance mode analysis. As shown in Figs. 7(a) and 7(b), we obtained a good agreement between the experimental and the calculated results for the resonance modes of each site. The anisotropic parameters are evaluated to be  $D/k_B = -0.24$  K and  $E/k_B = -0.07$  K for site 1 and  $D/k_B = -0.14$  K and  $E/k_B = -0.04$  K for site 2. The evaluated parameters of the on-site anisotropy are very close to those of  $[\text{Mn}(\text{hfac})_2](o\text{-Py-V})$  [25] and are considered to

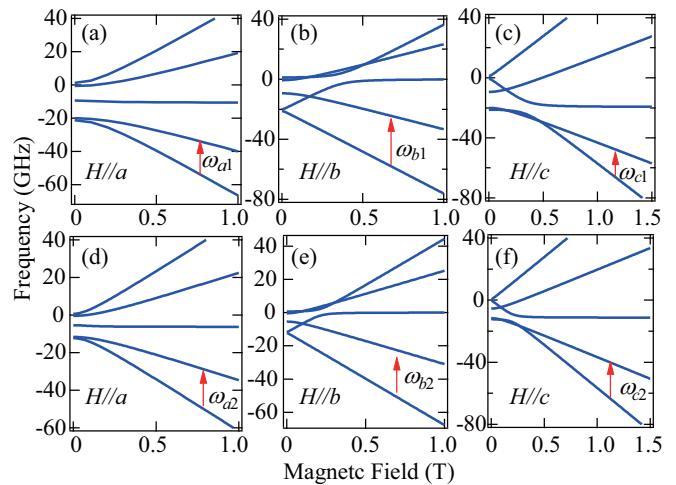


FIG. 8. Calculated energy branch of the  $S = 2$  hybrid spin with on-site biaxial anisotropy for (a–c) site 1 and (d–f) site 2. Arrows indicate spin-allowed transitions from the ground state.

originate from a magnetic dipole-dipole interaction and/or mixing of  $3d^5$  electronic states of the  $\text{Mn}^{2+}$  ion. As the ESR measurements were carried out at the sufficiently low temperature of 1.8 K, only the ESR transitions from the ground state were observed.

Figures 8(a)–8(c) and 8(d)–8(f) show the energy levels calculated by using the evaluated parameters for site 1 and site 2, respectively. Although the energy levels are strongly mixed because of the anisotropy and applied magnetic field, the ESR selection rule permits one resonance mode for each field direction at experimental fields higher than 1 T. The resonance modes for  $H\parallel a$ ,  $H\parallel b$ , and  $H\parallel c$  correspond to the transitions  $\omega_{ai}$ ,  $\omega_{bi}$ , and  $\omega_{ci}$  ( $i = 1, 2$ ) indicated by the arrows in the energy branches, respectively. For the easy-axis direction ( $H\parallel b$ ), the ground state and first excited state correspond to  $|-2\rangle$  and  $|-1\rangle$ , where the eigenstates are defined as  $|S_z\rangle$ , at the experimental fields, respectively.

As the metamagnetic phase transition occurs when the magnetic anisotropy is considerably larger than the exchange interactions, the absolute values of  $J_1$ ,  $J_2$ , and  $J_3$  forming the  $S = 2$  honeycomb lattice can be roughly estimated to be less than 0.1 K.

#### IV. SUMMARY

We have synthesized a Mn-verdazyl complex  $[\text{Mn}(\text{hfac})_2][o\text{-Py-V-(4-F)}_2]$ . Through analysis of the magnetic susceptibility and ESR spectra, we revealed that the strong intramolecular AF interaction between spins on  $\text{Mn}^{2+}$  and the verdazyl radical formed an  $S = 2$  hybrid spin below approximately 100 K. In the low-temperature regions, the magnetic susceptibility and specific heat indicated a phase transition to 3D order at  $T_N = 0.63$  K. The entropy change associated with the phase transition was almost one-third of the total magnetic entropy of  $S = 2$ , which indicated sufficient development of a short-range order in the  $S = 2$  2D honeycomb plane above  $T_N$ . Below  $T_N$ , we observed a metamagnetic phase transition on the  $S = 2$  honeycomb lattice with a large magnetic anisotropy. Furthermore, by analyzing the ESR modes,

we evaluated the on-site biaxial anisotropy responsible for the anisotropic magnetic behavior. Consequently, we demonstrated the realization of an  $S > 1/2$  spin system by using the metal-radical hybrid-spin approach in a verdazyl-based complex.

#### ACKNOWLEDGMENTS

This research was partly supported by Grant for Basic Science Research Projects from KAKENHI (No. 17H04850,

No. 18H01164, No. 19J01004, and No. 19H04550), Izumi Science and Technology Foundation, SEI Group CSR Foundation, and Nanotechnology Platform Program (Molecule and Material Synthesis) of the Ministry of Education, Culture, Sports, Science and Technology (MEXT), Japan. Part of this work was performed under the interuniversity cooperative research program of the joint-research program of ISSP, The University of Tokyo.

- [1] M. Takahashi, P. Turek, Y. Nakazawa, M. Tamura, K. Nozawa, D. Shiomi, M. Ishikawa, and M. Kinoshita, *Phys. Rev. Lett.* **67**, 746 (1991).
- [2] I. Takayuki, T. Hidenori, N. Takashi, Y. Hajime, Y. Masanori, I. Fujiko, I. Hiizu, T. Naoya, and I. Masayasu, *Chem. Lett.* **23**, 919 (1994).
- [3] K. Maekawa, D. Shiomi, T. Ise, K. Sato, and T. Takui, *Org. Biomol. Chem.* **5**, 1641 (2007).
- [4] T. Sugano, St. J. Blundell, T. Lancaster, F. L. Pratt, and H. Mori, *Phys. Rev. B* **82**, 180401(R) (2010).
- [5] J. Laugier, P. Rey, C. Benelli, D. Gatteschi, and C. Zanchini, *J. Am. Chem. Soc.* **108**, 6931 (1986).
- [6] K. Inoue, T. Hayamizu, H. Iwamura, D. Hashizumi, and Y. Ohashi, *J. Am. Chem. Soc.* **118**, 1803 (1996).
- [7] C. Train, L. Norel, and M. Baumgarten, *Coord. Chem. Rev.* **253**, 2342 (2009).
- [8] I. Dasna, S. Golhen, L. Ouahab, N. Daro, and J.-P. Sutter, *Polyhedron* **20**, 1371 (2001).
- [9] M. Nihei, T. Maeshima, and Y. Kose, and H. Oshio, *Polyhedron* **26**, 1993 (2007).
- [10] D.-Z. Gao, Y.-Q. Sun, D.-Z. Liao, Z.-H. Jiang, and S.-P. Yan, *Z. Anorg. Allg. Chem.* **634**, 1950 (2008).
- [11] A. Okazawa, Y. Nagaichi, T. Nogami, and T. Ishida, *Inorg. Chem.* **47**, 8859 (2008).
- [12] A. Okazawa and T. Ishida, *Inorg. Chem.* **49**, 10144 (2010).
- [13] B. D. Koivisto and R. G. Hicks, *Coord. Chem. Rev.* **249**, 2612 (2005).
- [14] C. W. Johnston, S. D. J. McKinnon, B. O. Patrick, and R. G. Hicks, *Dalton Trans.* **42**, 16829 (2013).
- [15] T. M. Barclay, R. G. Hicks, M. T. Lemaire, and L. K. Thompson, *Inorg. Chem.* **40**, 5581 (2001).
- [16] S. D. J. McKinnon, B. O. Patrick, A. B. P. Lever, and R. G. Hicks, *Inorg. Chem.* **52**, 8053 (2013).
- [17] D. J. R. Brook, V. Lynch, C. Conklin, and M. A. Fox, *J. Am. Chem. Soc.* **119**, 5155 (1997).
- [18] H. Yamaguchi, K. Iwase, T. Ono, T. Shimokawa, H. Nakano, Y. Shimura, N. Kase, S. Kittaka, T. Sakakibara, T. Kawakami, and Y. Hosokoshi, *Phys. Rev. Lett.* **110**, 157205 (2013).
- [19] H. Yamaguchi, A. Toho, K. Iwase, T. Ono, T. Kawakami, T. Shimokawa, A. Matsuo, and Y. Hosokoshi, *J. Phys. Soc. Jpn.* **82**, 043713 (2013).
- [20] H. Yamaguchi, T. Okubo, K. Iwase, T. Ono, Y. Kono, S. Kittaka, T. Sakakibara, A. Matsuo, K. Kindo, and Y. Hosokoshi, *Phys. Rev. B* **88**, 174410 (2013).
- [21] H. Yamaguchi, H. Miyagai, M. Yoshida, M. Takigawa, K. Iwase, T. Ono, N. Kase, K. Araki, S. Kittaka, T. Sakakibara, T. Shimokawa, T. Okubo, K. Okunishi, A. Matsuo, and Y. Hosokoshi, *Phys. Rev. B* **89**, 220402 (2014).
- [22] H. Yamaguchi, H. Miyagai, T. Shimokawa, K. Iwase, T. Ono, Y. Kono, N. Kase, K. Araki, S. Kittaka, T. Sakakibara, T. Kawakami, K. Okunishi, and Y. Hosokoshi, *J. Phys. Soc. Jpn.* **83**, 033707 (2014).
- [23] H. Yamaguchi, T. Okubo, S. Kittaka, T. Sakakibara, K. Araki, K. Iwase, N. Amaya, T. Ono, and Y. Hosokoshi, *Sci. Rep.* **5**, 15327 (2015).
- [24] H. Yamaguchi, Y. Shinpuku, T. Shimokawa, K. Iwase, T. Ono, Y. Kono, S. Kittaka, T. Sakakibara, and Y. Hosokoshi, *Phys. Rev. B* **91**, 085117 (2015).
- [25] H. Yamaguchi, Y. Shinpuku, Y. Kono, S. Kittaka, T. Sakakibara, M. Hagiwara, T. Kawakami, K. Iwase, T. Ono, and Y. Hosokoshi, *Phys. Rev. B* **93**, 115145 (2016).
- [26] H. Yamaguchi, M. Okada, Y. Kono, S. Kittaka, T. Sakakibara, T. Okabe, Y. Iwasaki, and Y. Hosokoshi, *Sci. Rep.* **7**, 16144 (2017).
- [27] N. Uemoto, Y. Kono, S. Kittaka, T. Sakakibara, T. Yajima, Y. Iwasaki, S. Miyamoto, Y. Hosokoshi, and H. Yamaguchi, *Phys. Rev. B* **99**, 094418 (2019).
- [28] M. Oshikawa, *J. Phys. Condens. Matter* **4**, 7469 (1992).
- [29] H. Aschauer and U. Schollwöck, *Phys. Rev. B* **58**, 359 (1998).
- [30] T. Tonegawa, K. Okamoto, H. Nakano, T. Sakai, K. Nomura, and M. Kaburagi, *J. Phys. Soc. Jpn.* **80**, 043001 (2011).
- [31] K. Okamoto, T. Tonegawa, H. Nakano, T. Sakai, K. Nomura, and M. Kaburagi, *J. Phys.: Conf. Ser.* **302**, 012014 (2011).
- [32] Y.-C. Tzeng, *Phys. Rev. B* **86**, 024403 (2012).
- [33] J. A. Kjäll, M. P. Zaletel, R. S. K. Mong, J. H. Bardarson, and F. Pollmann, *Phys. Rev. B* **87**, 235106 (2013).
- [34] Y. Kono, T. Okabe, N. Uemoto, Y. Iwasaki, Y. Hosokoshi, S. Kittaka, T. Sakakibara, and H. Yamaguchi, *Phys. Rev. B* **101**, 014437 (2020).
- [35] K. Takano, *Phys. Rev. B* **74**, 140402(R) (2006).
- [36] W. Li, S.-S. Gong, Y. Zhao, and G. Su, *Phys. Rev. B* **81**, 184427 (2010).
- [37] Y.-Z. Huang, B. Xi, X. Chen, W. Li, Z.-C. Wang, and G. Su, *Phys. Rev. E* **93**, 062110 (2016).
- [38] M. C. Burla, R. Caliandro, M. Camalli, B. Carrozzini, G. L. Cascarano, L. De Caro, C. Giacovazzo, G. Polidori, and R. Spagna, *J. Appl. Cryst.* **38**, 381 (2005).
- [39] G. M. Sheldrick, *SHELXL97, Program for Crystal Structure Determination* (University of Göttingen, Göttingen, Germany, 1997).
- [40] T. Kawakami, Y. Kitagawa, F. Matsuoka, Y. Yamashita, and K. Yamaguchi, *Polyhedron* **20**, 1235 (2001).